Supplementary Materials

Revisiting the Bøggild Intergrowth in the Iridescent Labradorite Feldspars: Ordering, Kinetics, and Phase Equilibria

Shiyun Jin[1,2], Huifang Xu*[1], and Seungyeol Lee[1,3,4]

1. Department of Geoscience, University of Wisconsin-Madison, 1215 W. Dayton Street, Madison, WI 53706, USA.

2. Gemological Institute of America, 5355 Armada Drive, Carlsbad, California 92008, USA

3. USRA Lunar and Planetary Institute, 3600 Bay Area Boulevard, Houston, TX 77058, USA

4. Astromaterials Research and Exploration Directorate, NASA Johnson Space Center, 2101 NASA Parkway, Houston, TX 77058, USA

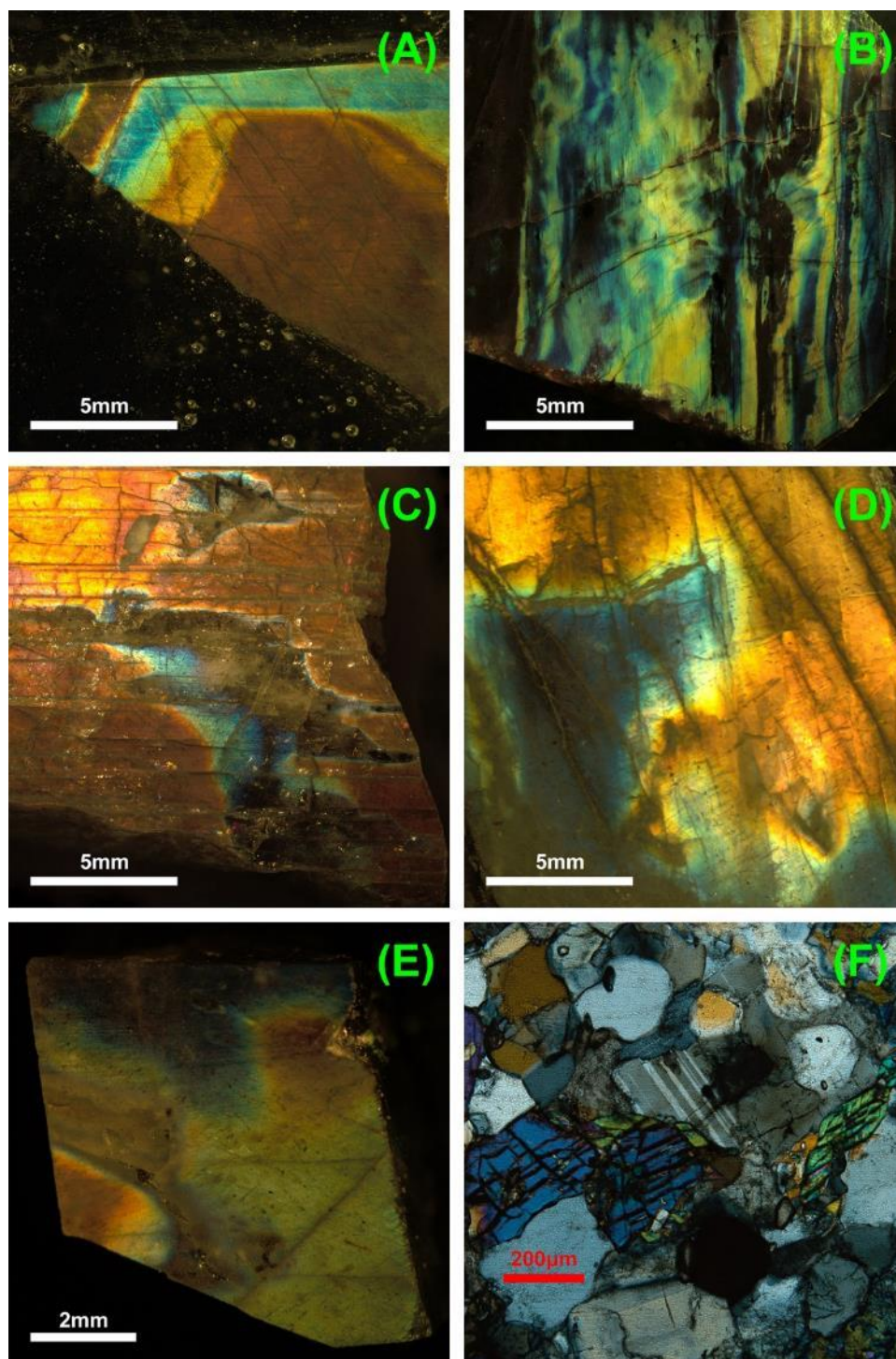* Corresponding author: hfxu@geology.wisc.edu

Figure S1 Optical images of the samples studied in this paper. (A) sample Gem118 from Finland; (B) sample VB (Volga Blue) from Ukraine; (C) sample R2923 from Sweden; (D) sample MAD from Madagascar. (E) sample Gem113 from Labrador, Canada; (F) thin section of sample 987L, transmitted cross-polarized light.
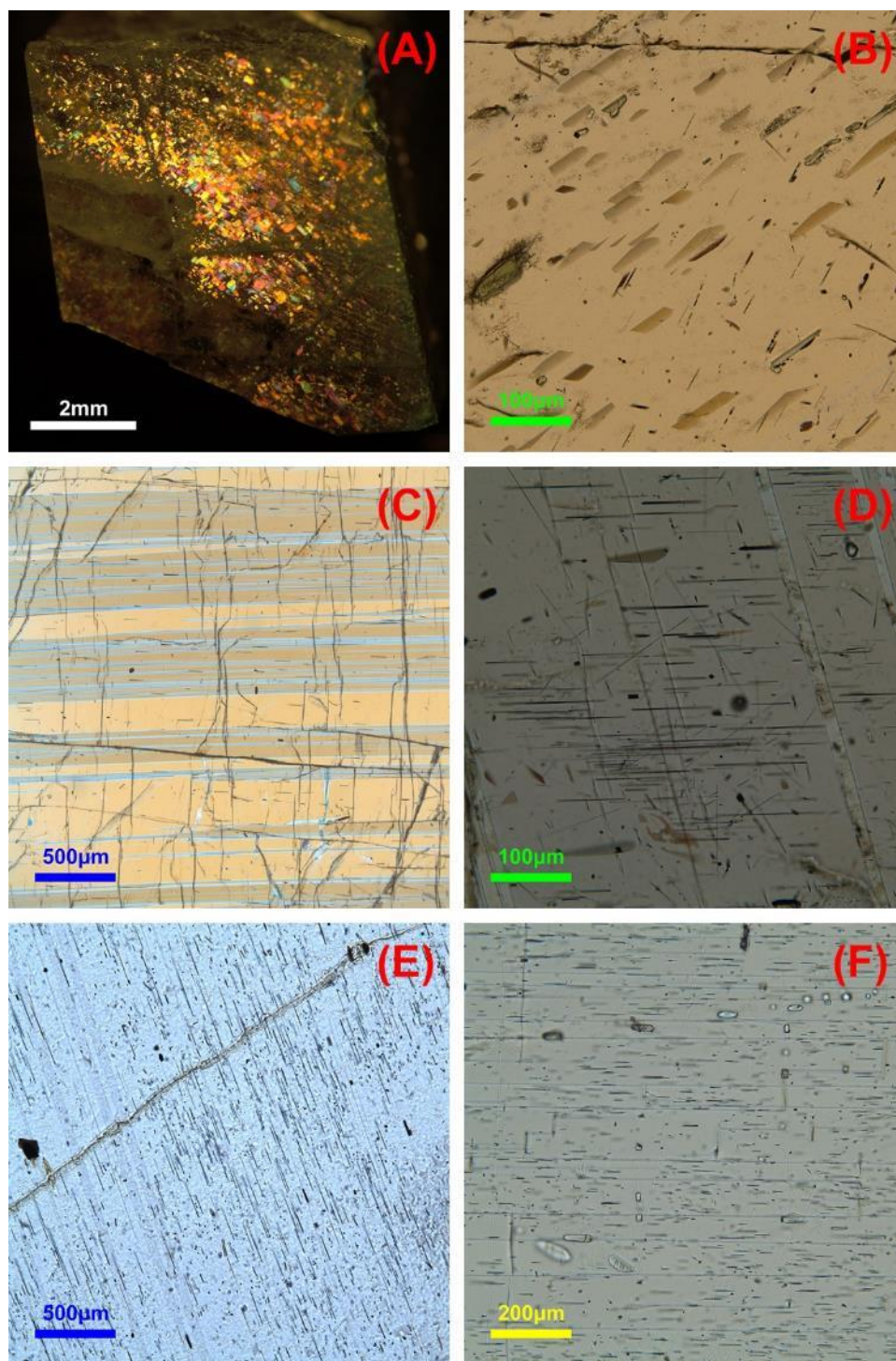
Figure S2 Optical images of the igneous samples studied in this paper showing the inclusions. (A) brilliant reflections from the flaky inclusions inside Gem113 with light shined from a different angle as in Figure S1E; (B) flaky and needle-like inclusions in thin section of sample Gem113; (C) thin section of sample MAD with a few acicular inclusions; (D) thin section of sample R2923; (E) thin section of sample VB with high density acicular inclusions; (F) thin section of sample Gem118 with acicular inclusions and fluid inclusions.
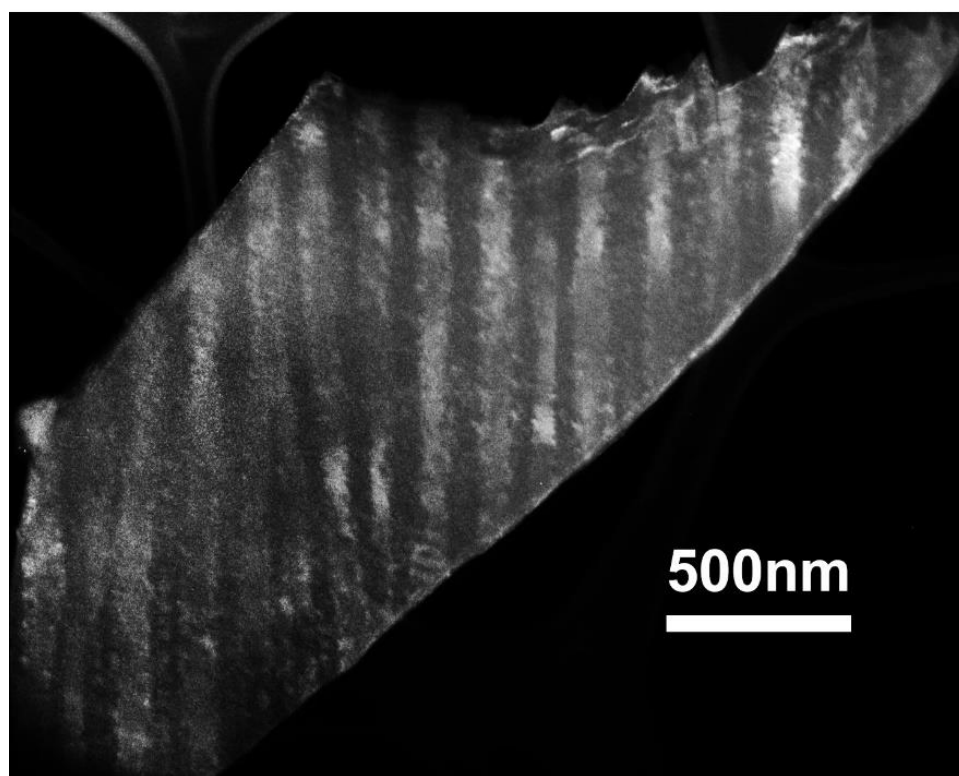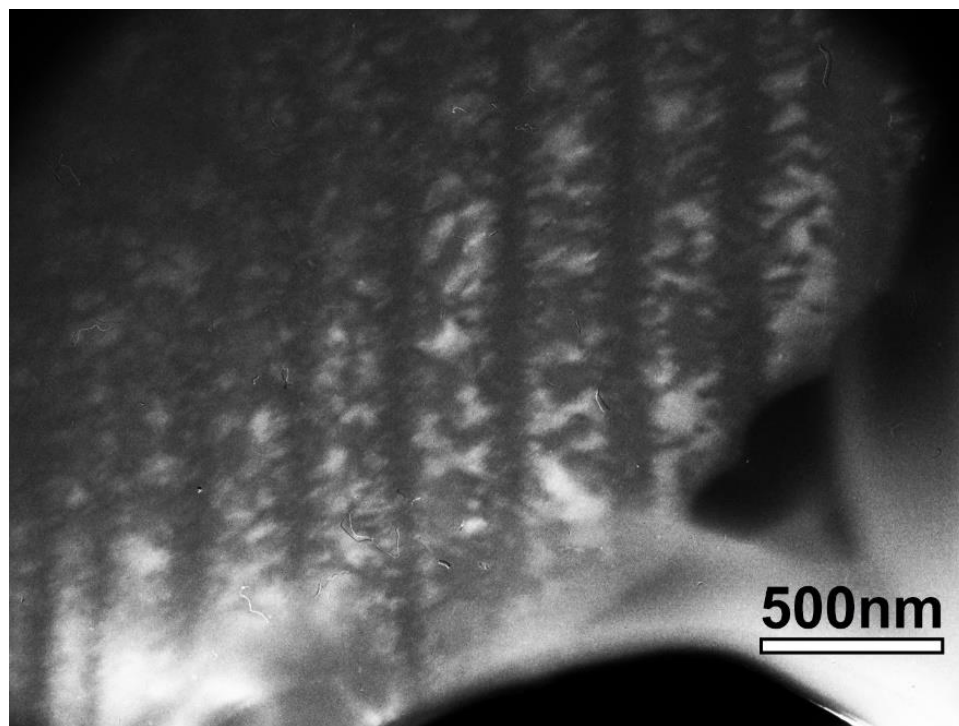
Figure S3 Dark field TEM images of the red-iridescent (top) and the blue-iridescent (bottom) areas in sample Gem118 from Finland. The contrast in the lamellae is resulted from out-of-phase boundary among the neighboring domains of the modulated structure.
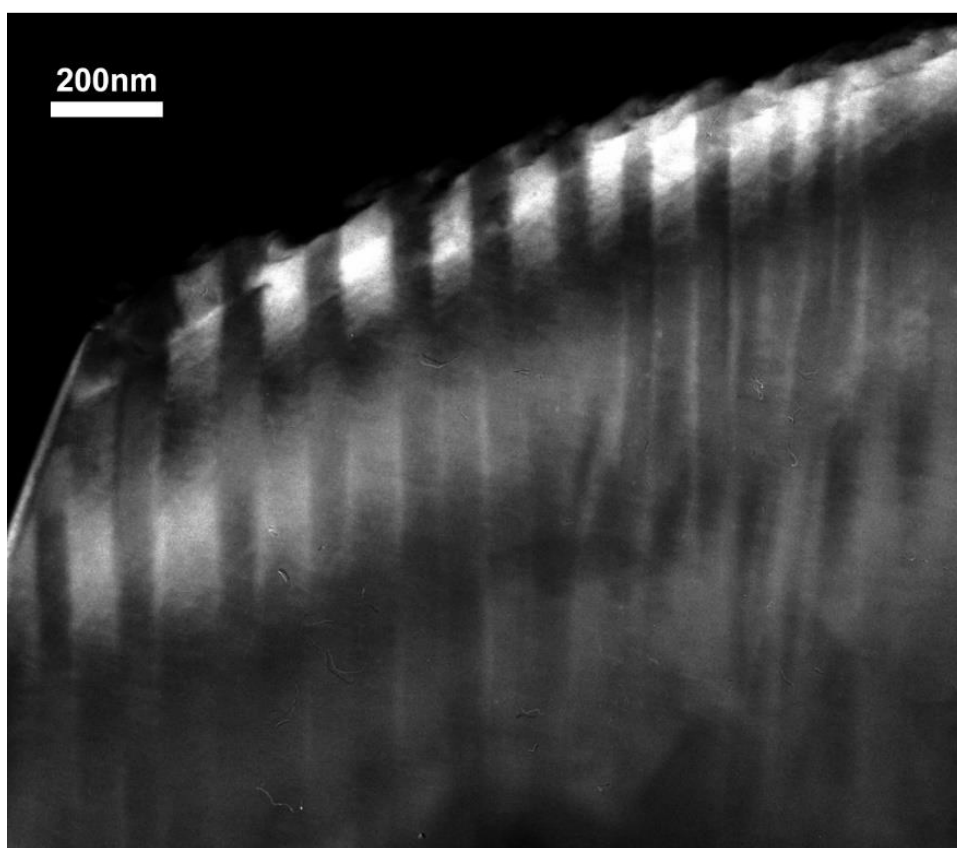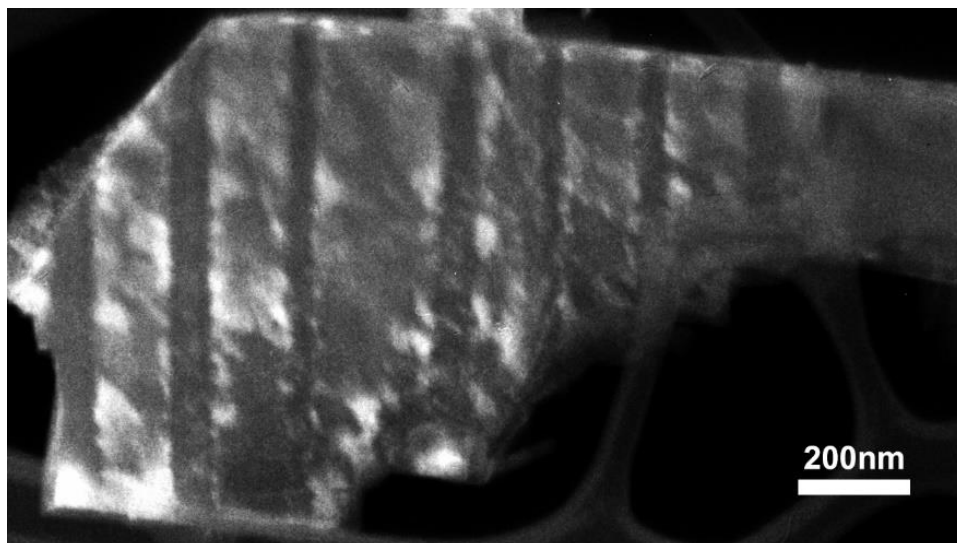
Figure S4 Dark field images showing exsolution lamellae of the red-iridescent area (top) and the blue-iridescent area (bottom) in sample Gem113 from Labrador, Canada.
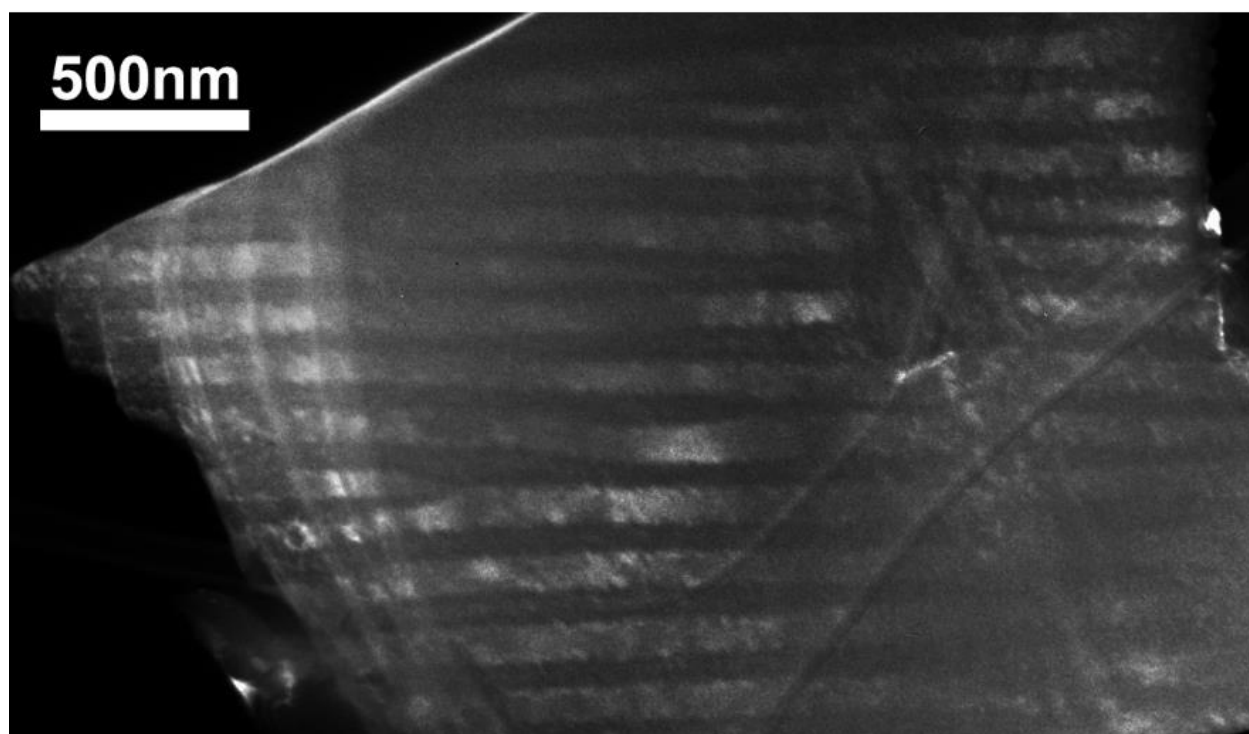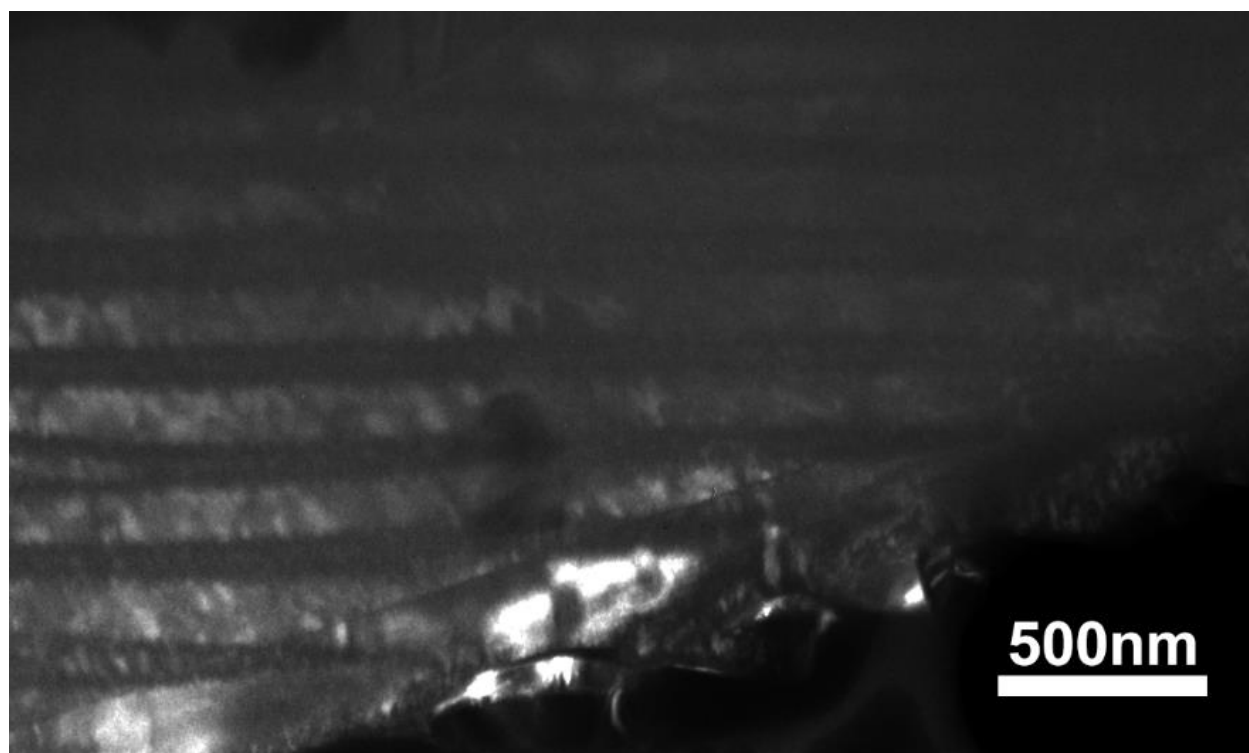
Figure S5 Dark field images showing exsolution lamellae of the orange-iridescent area (top) and the blue-iridescent area (bottom) in sample MAD from Madagascar.
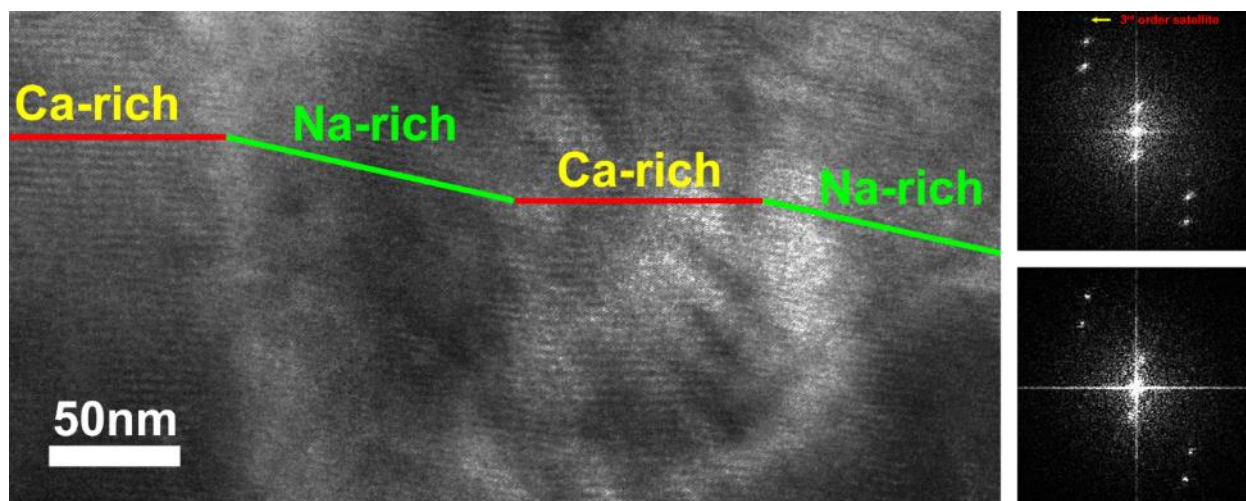
Figure S6 High-resolution TEM image of the blue-iridescent MAD sample, along with the FFT of selected area in each individual lamella. The difference in the modulation orientation is ~12°, which is smaller than the difference in the blue Gem113 sample as shown in Figure 1.
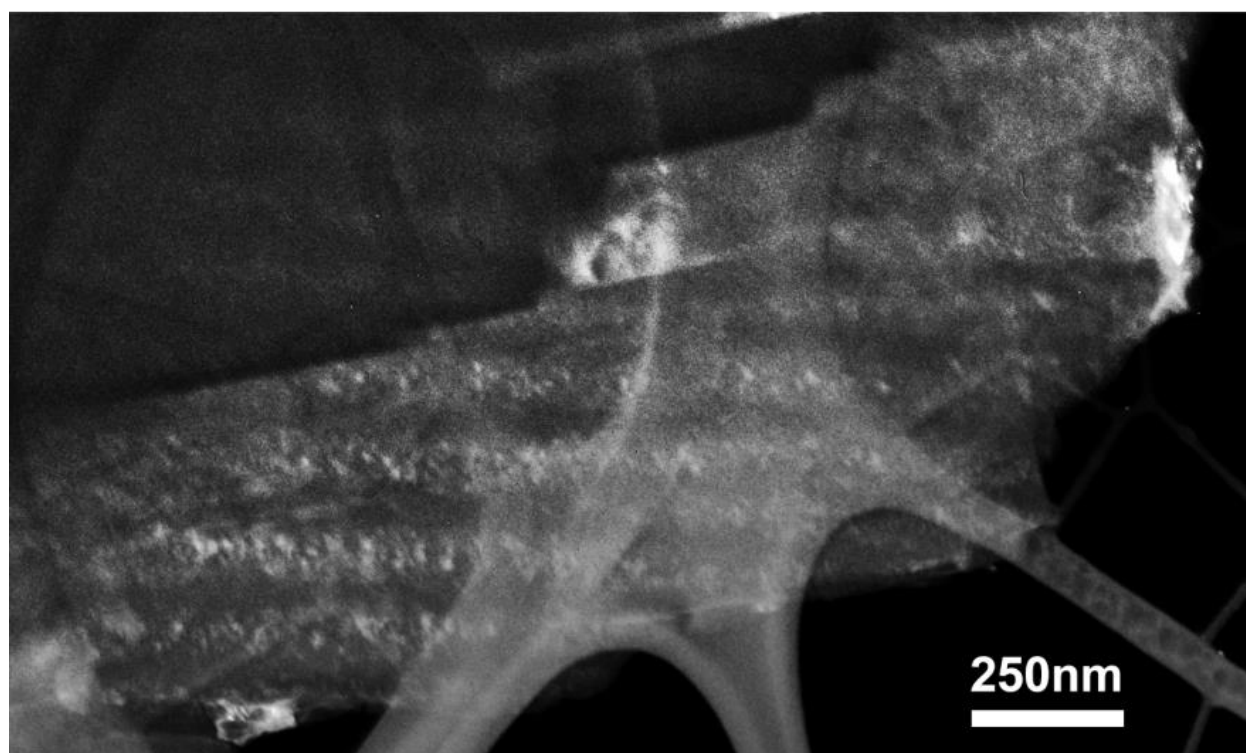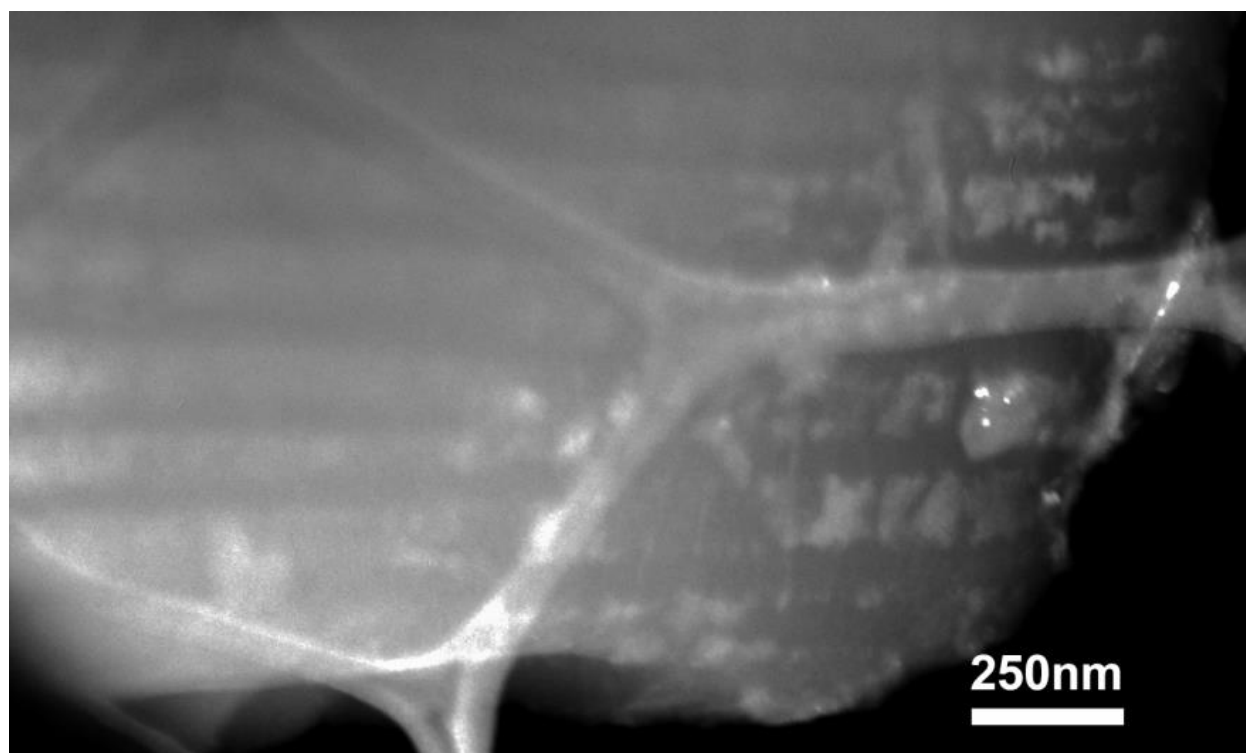
Figure S7 Dark-field images of the yellow (top) and green-blue (bottom) area in sample VB. The lamellae texture is very similar to the other samples as shown in Figures 2-4.
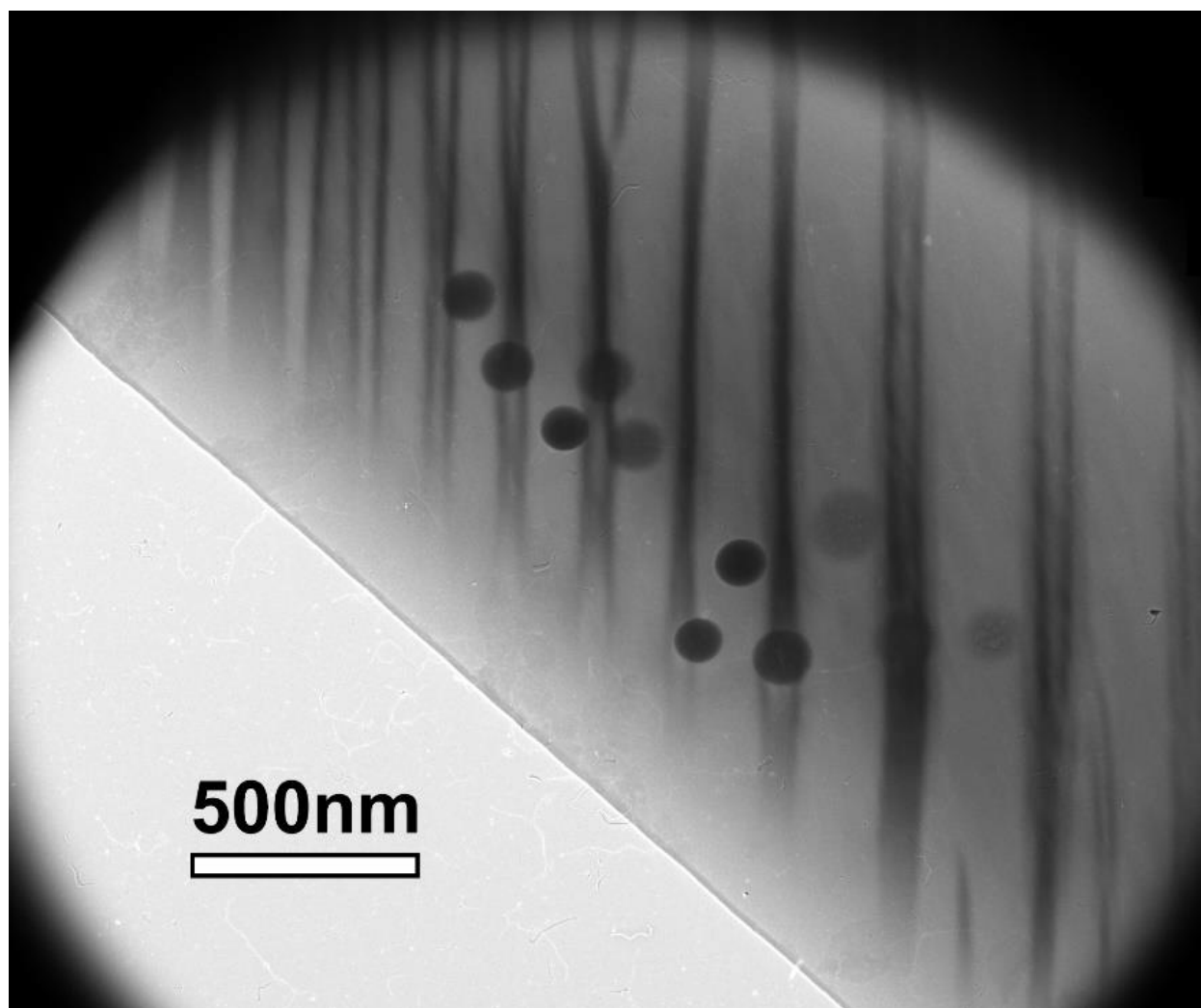
Figure S8 Bright-field TEM image of sample 987L, showing exsolution lamellae of various thickness. The wider lamellae are Ca-rich and thinner ones Na-rich. The dark circles are left by focused electron beams for collection EDS spectrum.
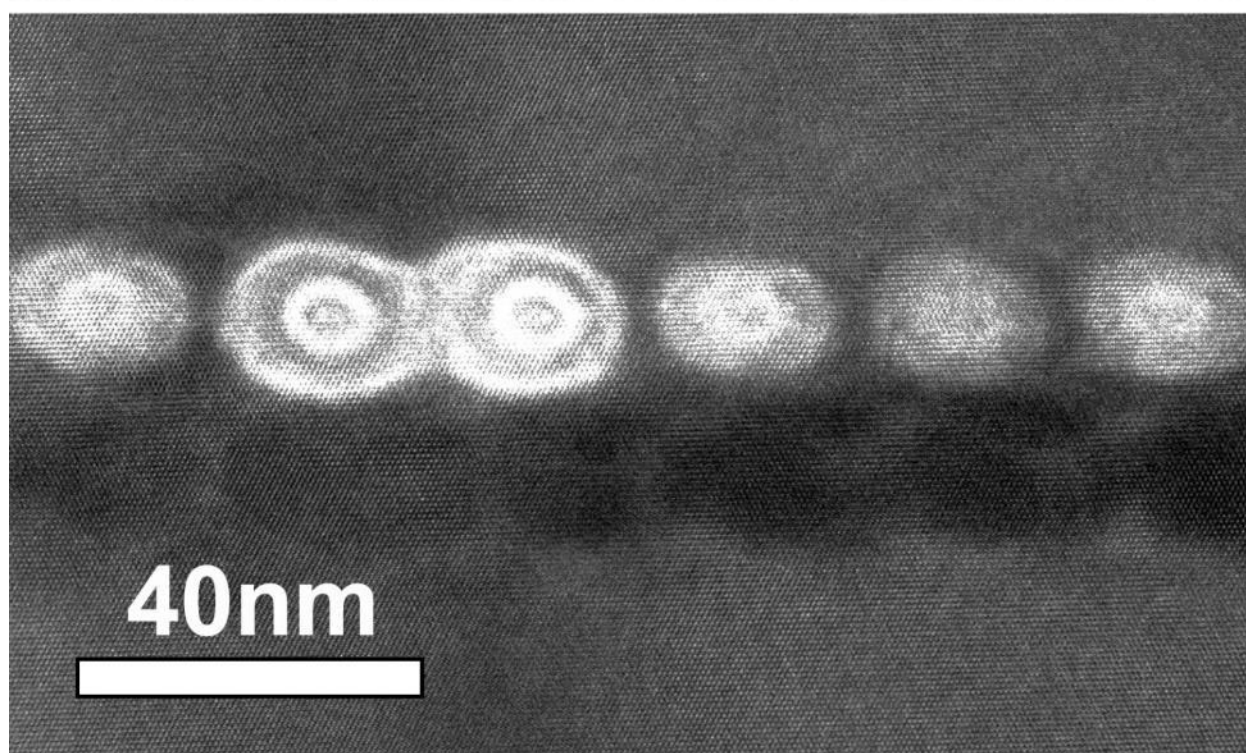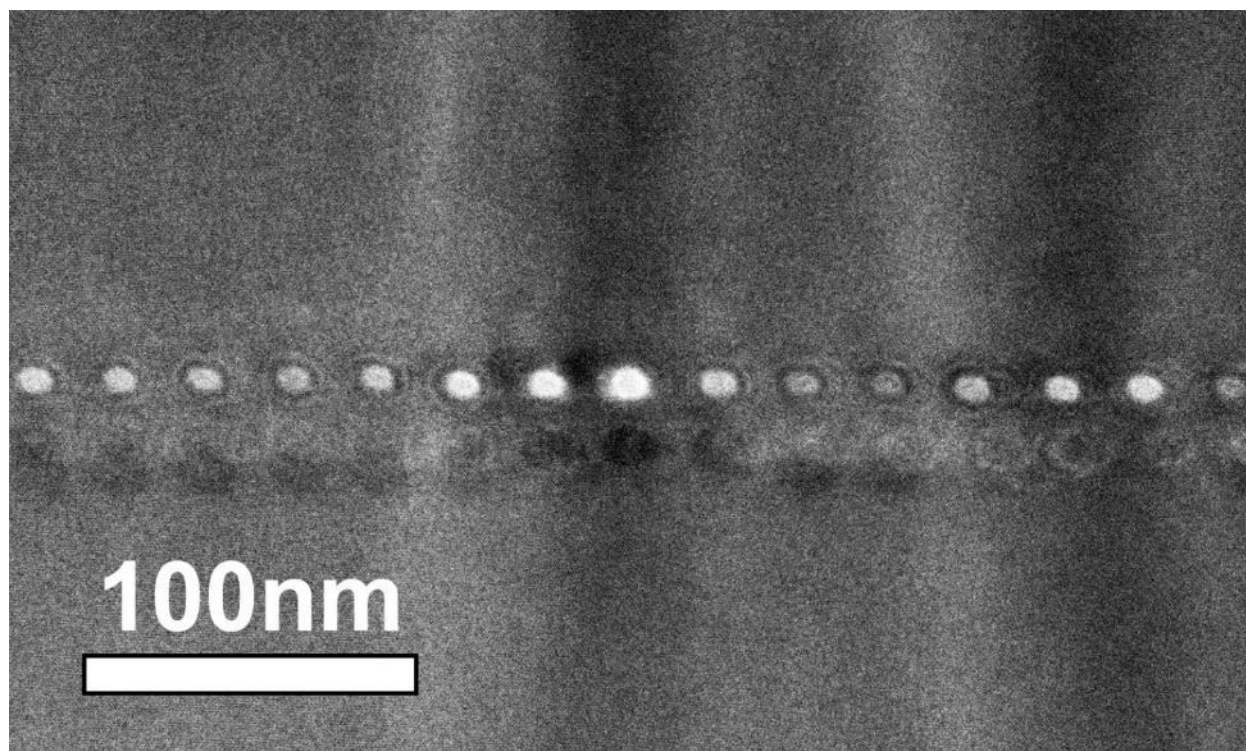
Figure S9 High resolution TEM image of sample 987L after collecting EDS data along the traverse. The equally spaced bright dots are the marks left by the focused electron beam. The damage zone as shown in the image is larger than the electron beam itself, and may interfere with one another, which makes the data not reliable for quantitive analysis for lamellae composition.
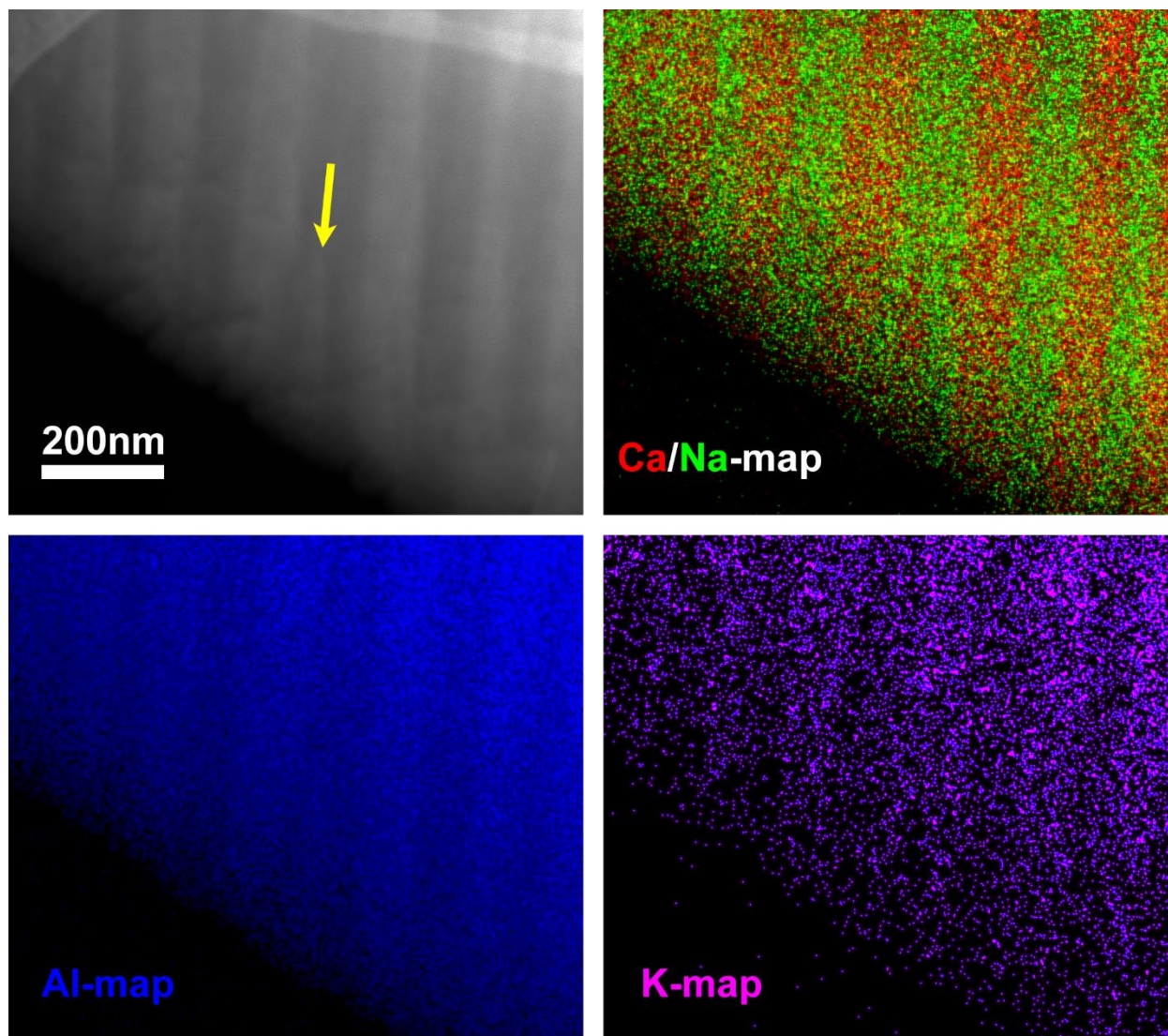
Figure S10 The HAADF STEM image of the blue Gem118 sample, along with the elemental maps of Ca, Na, Al, and K from the EDS map. Ca and Na are shown in the same map to enhance the contrast. The EDS map matches the STEM image perfectly, with Ca-rich lamellae brighter in the image, richer in Al and poorer in K. Even though the maps are much noisier than the STEM image, the show the same textures as in the STEM image.
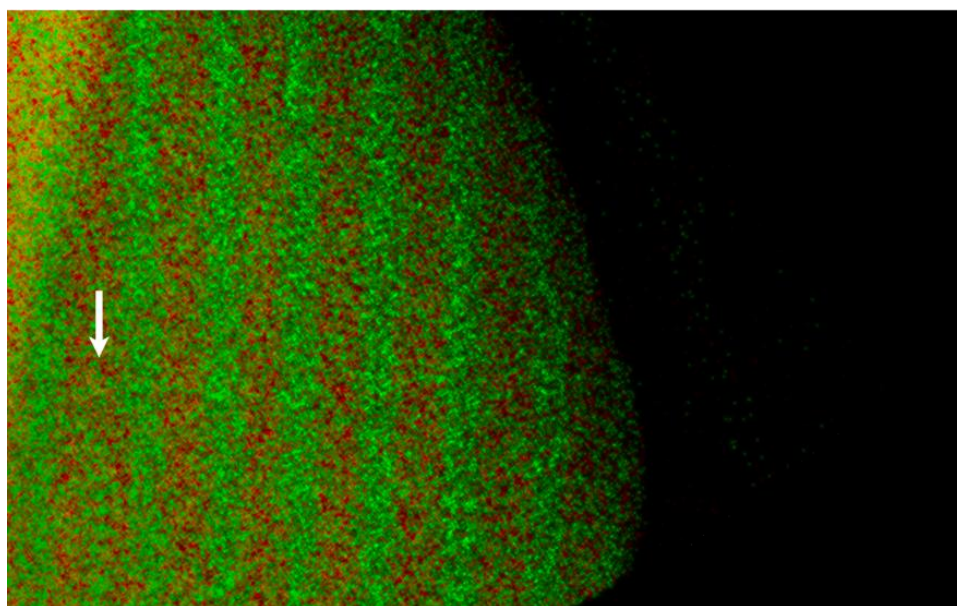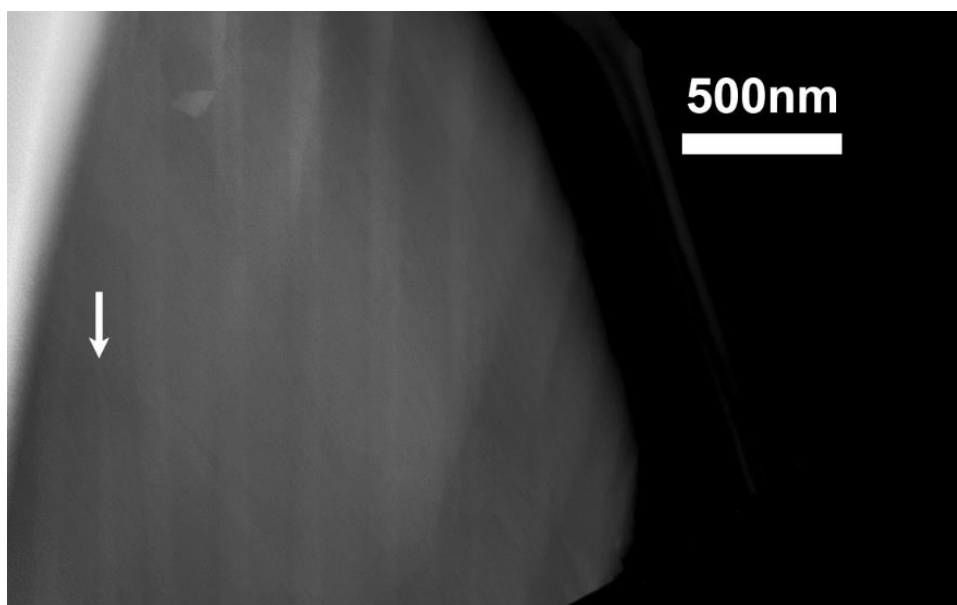
Figure S11 The HAADF STEM image and Ca/Na elemental map of the red Gem118 sample. The STEM image shows some strange contrast that does not correspond to the chemical composition, most likely resulting from some elastically scattered signals. Signals of Ca/Na counts in the EDS map are much better at showing the chemical differences between lamellae.
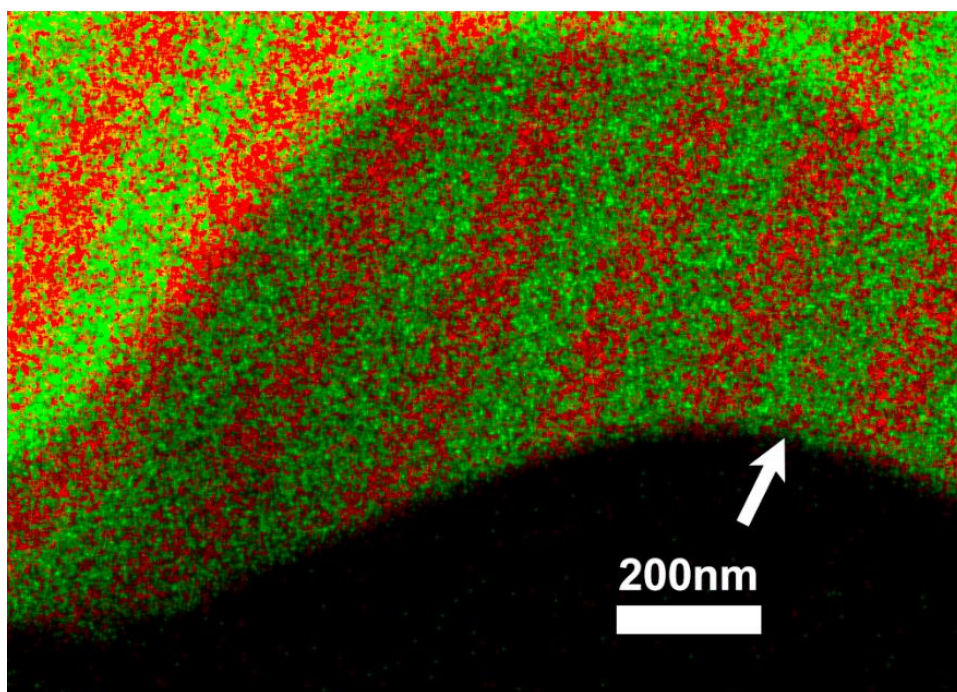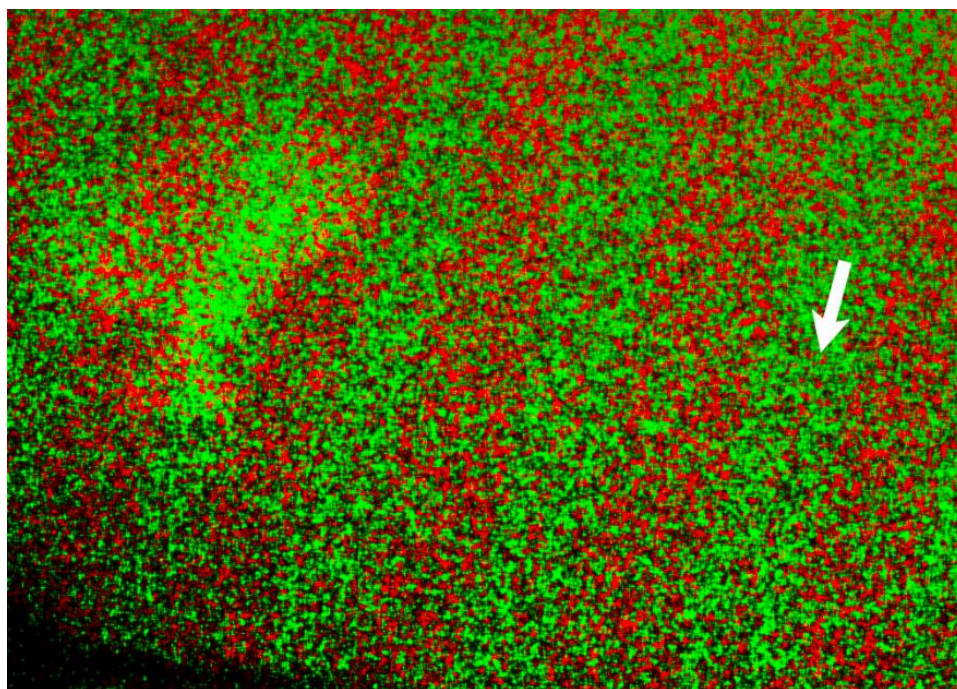
Figure S12 EDS maps of the red (top) and blue (bottom) areas in sample R2923. The lamellae thickness is very similar to that of sample Gem113. The contrast is also higher in the blue area than in the red, indicating larger chemical differences between Ca-rich and Na-rich lamellae in blue sample. The red lines in the center of Na-rich lamellae are also marked by white arrows.
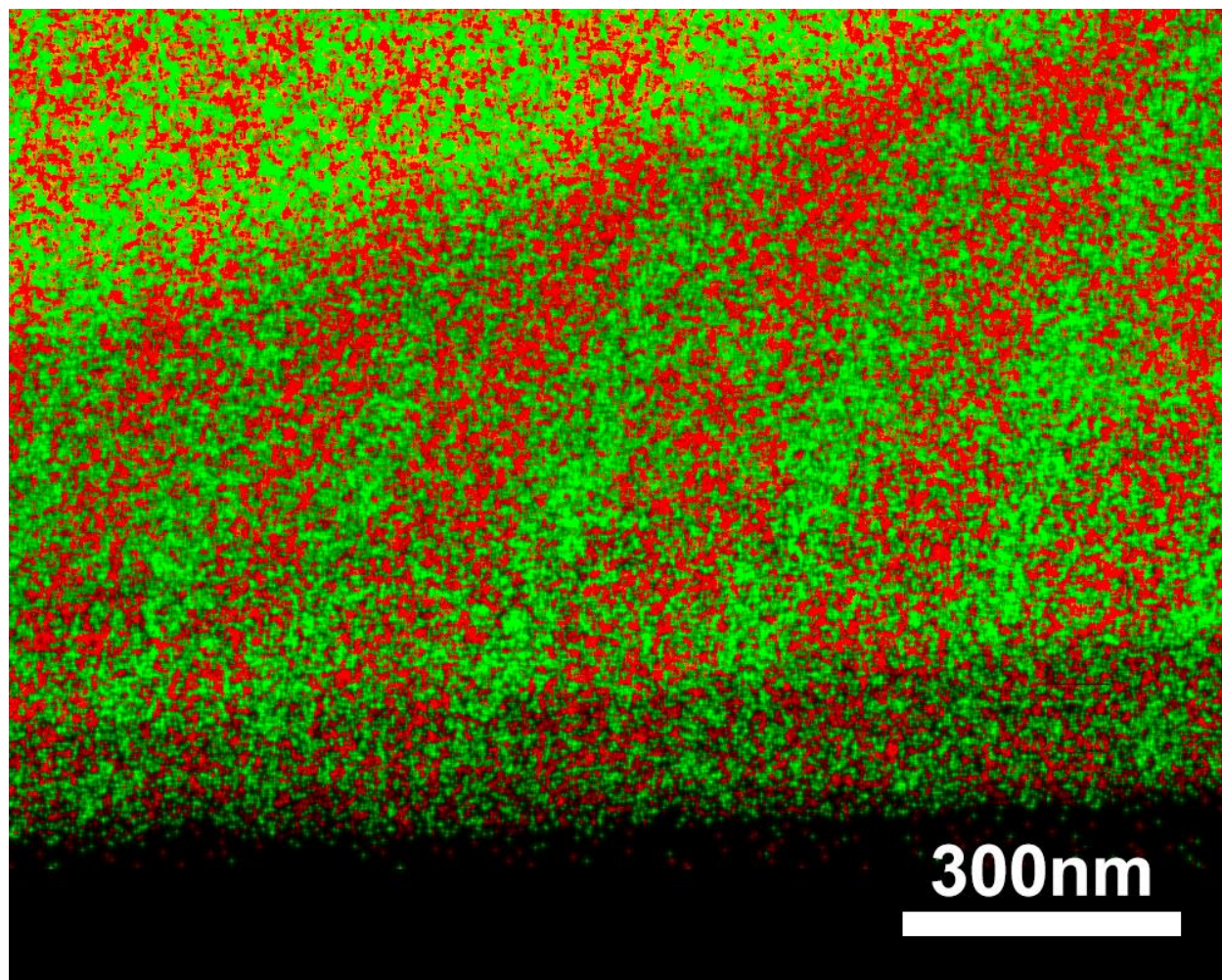
Figure S13 EDS map of the yellow VB sample. The volume ratio between Ca-rich and Na-rich lamellae is more than 2:1, even higher than the ratio in the red area of the other samples (MAD, R2923, Gem113, Gem118).
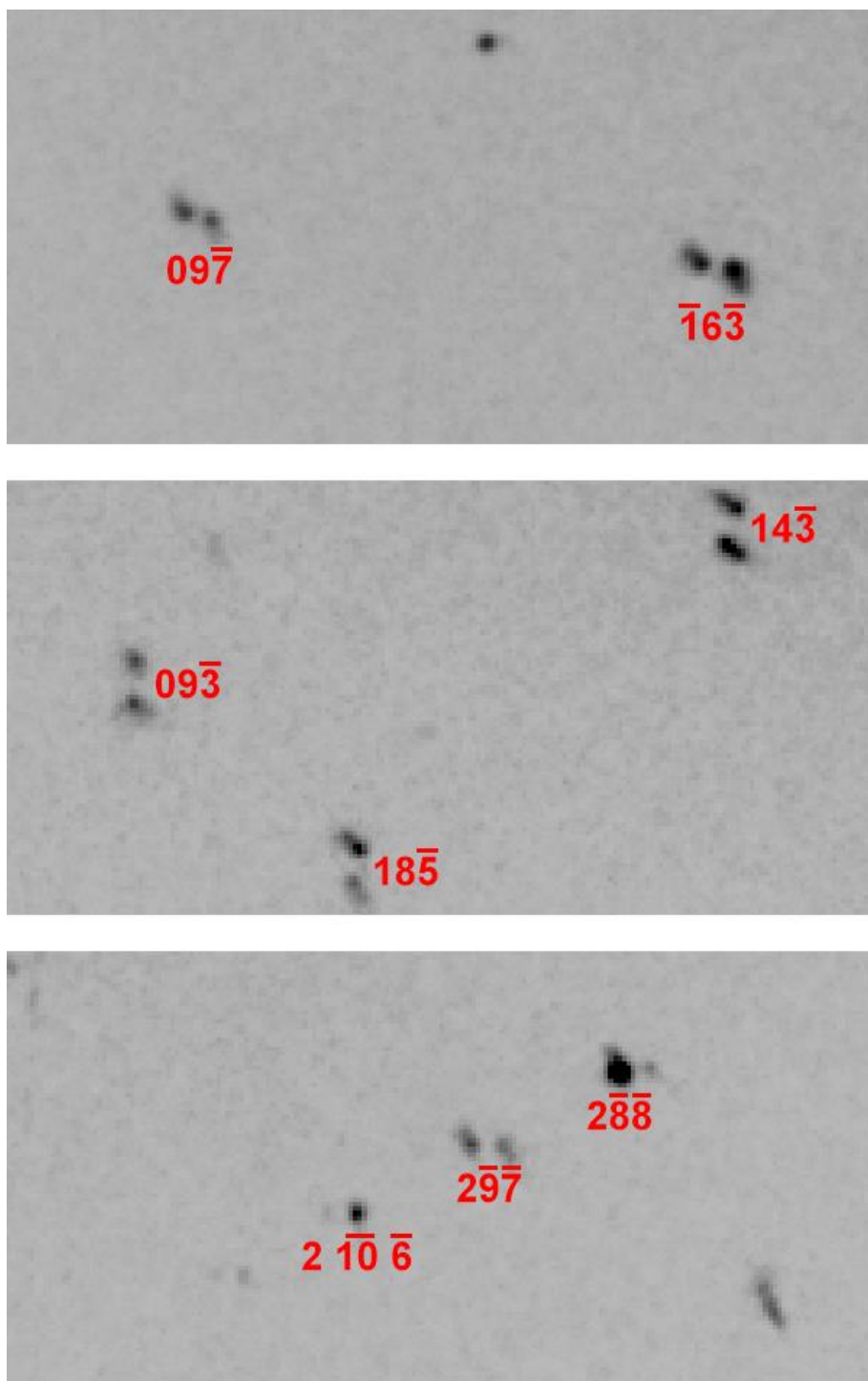
Figure S14 Selected frames from the single-crystal diffraction data of the red Gem118 sample. Two sets of *e*-reflection pairs are obviously shown in these frames. This is a very unique feature of the red Gem118 sample. All the other samples, even though also consisting of two phases of different compositions, show only one set of satellite reflections in the X-ray diffraction pattern. The indexing is based on anorthite cell.
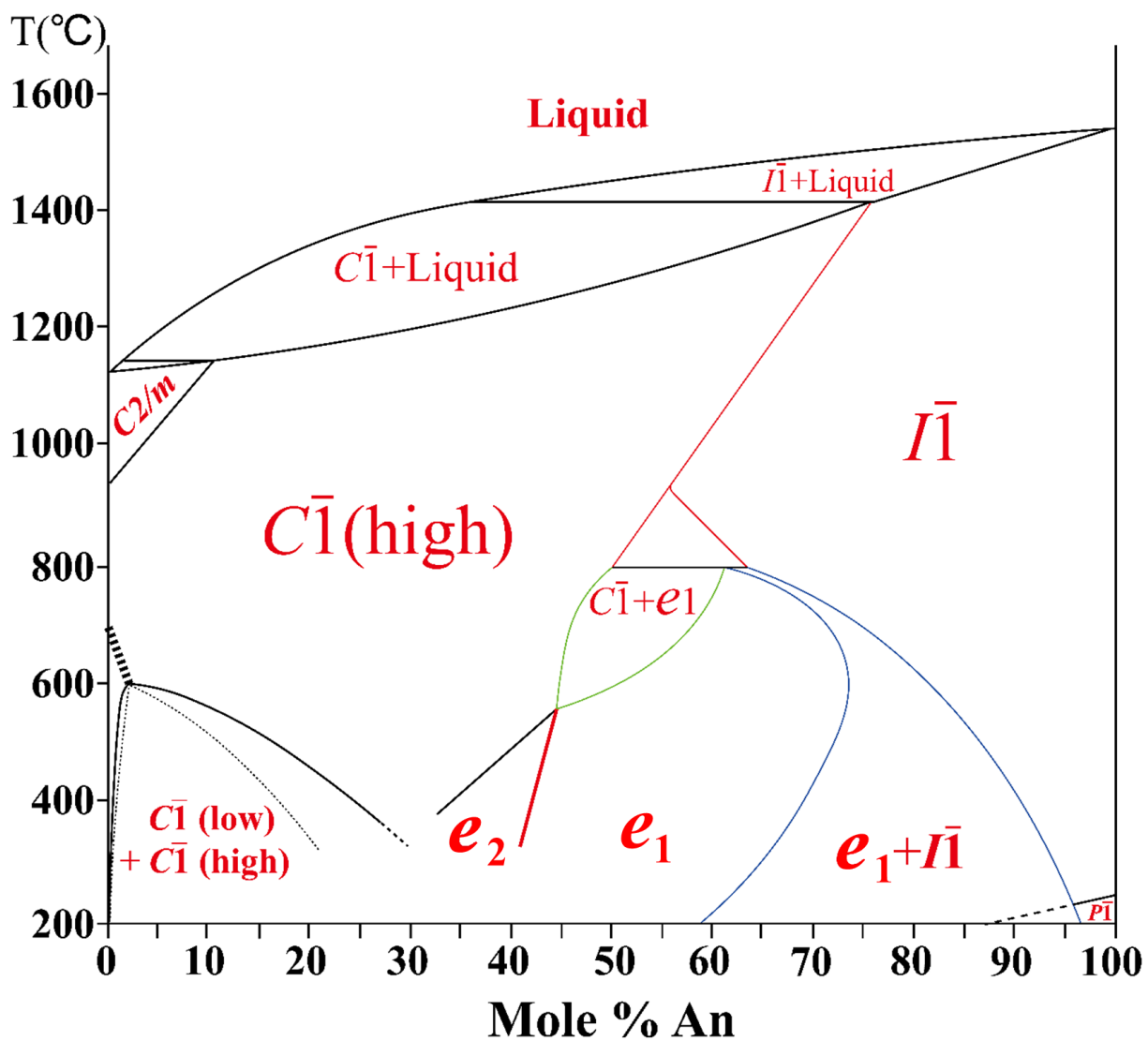
Figure S15 A complete binary phase diagram of the plagioclase feldspar with the topology shown in Figure 12*c*. The rest of the phase diagram would be the same for the other two topologies in Figure 12, mostly following Carpenter (1994).

Figure S16 List of plagioclase phase diagrams (Smith 1974, 1986; McConnell 1974, 2008; Nord *et al.* 1974; Grove *et al.* 1983, 1986; Ribbe, 1987; Carpenter 1994; Vinograd *et al.* 2001).

Table S1 Electron microprobe analyses results of the plagioclase samples studied in this paper.

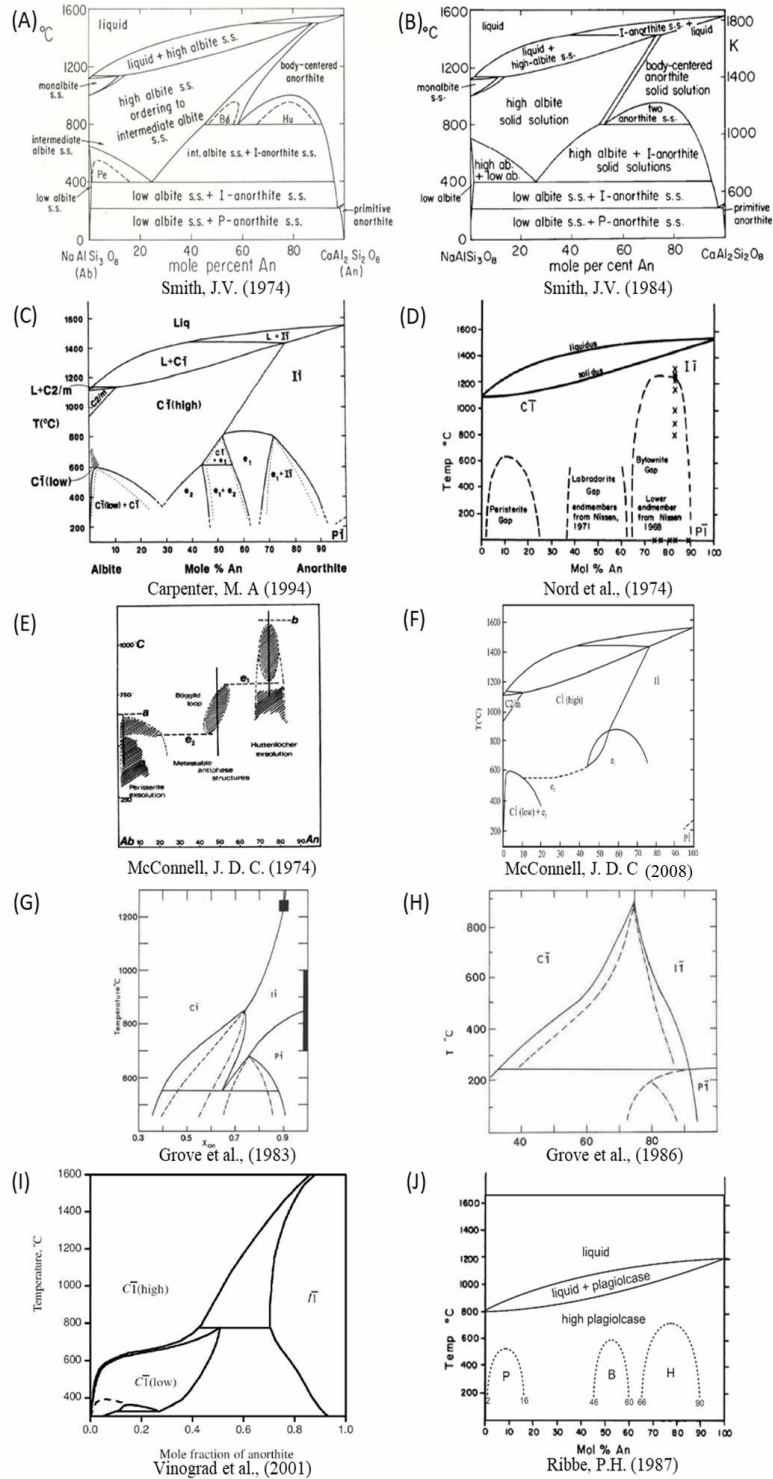| Sample	Oxide Weight%							Formula normalized to 8 oxygen							Composition
	SiO_2	Al_2O_3	FeO	CaO	Na_2O	K_2O	Total	Si	Al	Fe	Ca	Na	K	Total	
987L	54.888	28.065	0.088	10.009	5.958	0.129	99.136	2.494	1.503	0.003	0.487	0.525	0.007	13.020	$An_{47.8}Ab_{51.5}Or_{0.7}$
	54.793	28.418	0.019	10.017	6.022	0.121	99.390	2.484	1.518	0.001	0.486	0.529	0.007	13.025	$An_{47.6}Ab_{51.8}Or_{0.7}$
	54.343	28.500	0.013	9.999	5.986	0.157	98.998	2.474	1.529	0.001	0.488	0.528	0.009	13.030	$An_{47.6}Ab_{51.5}Or_{0.9}$
	55.167	28.101	0.008	9.585	6.156	0.088	99.106	2.503	1.503	0.000	0.466	0.542	0.005	13.019	$An_{46.0}Ab_{53.5}Or_{0.5}$
	55.268	28.413	0.052	9.918	5.891	0.108	99.650	2.495	1.512	0.002	0.480	0.516	0.006	13.010	$An_{47.9}Ab_{51.5}Or_{0.6}$
	54.421	28.519	0.056	10.218	5.896	0.102	99.212	2.473	1.528	0.002	0.498	0.520	0.006	13.026	$An_{48.6}Ab_{50.8}Or_{0.6}$
	54.911	28.340	0.054	10.103	5.871	0.120	99.399	2.488	1.513	0.002	0.490	0.516	0.007	13.017	$An_{48.4}Ab_{50.9}Or_{0.7}$
	54.524	28.625	0.045	10.066	5.939	0.106	99.305	2.474	1.531	0.002	0.489	0.523	0.006	13.025	$An_{48.1}Ab_{51.3}Or_{0.6}$
	54.414	28.504	0.022	10.399	5.555	0.161	99.055	2.475	1.528	0.001	0.507	0.490	0.009	13.010	$An_{50.4}Ab_{48.7}Or_{0.9}$
	53.946	28.984	0.061	10.588	5.562	0.091	99.233	2.452	1.553	0.002	0.516	0.490	0.005	13.019	$An_{51.0}Ab_{48.5}Or_{0.5}$
	54.155	28.890	0.041	10.455	5.762	0.078	99.381	2.458	1.545	0.002	0.508	0.507	0.005	13.025	$An_{49.8}Ab_{49.7}Or_{0.4}$
	54.304	29.381	0.007	10.820	5.345	0.086	99.943	2.449	1.562	0.000	0.523	0.467	0.005	13.006	$An_{52.5}Ab_{47.0}Or_{0.5}$
MAD-orange	54.634	28.958	0.142	10.663	5.001	0.519	99.917	2.467	1.541	0.005	0.516	0.438	0.030	12.997	$An_{52.4}Ab_{44.5}Or_{3.0}$
	55.139	28.577	0.053	10.824	5.040	0.499	100.132	2.483	1.517	0.002	0.522	0.440	0.029	12.993	$An_{52.7}Ab_{44.4}Or_{2.9}$
	55.076	28.441	0.152	10.700	5.176	0.446	99.990	2.485	1.512	0.006	0.517	0.453	0.026	12.998	$An_{51.9}Ab_{45.5}Or_{2.6}$
	54.893	28.515	0.018	11.029	5.097	0.431	99.982	2.478	1.517	0.001	0.533	0.446	0.025	12.999	$An_{53.1}Ab_{44.4}Or_{2.5}$
MAD-yellow	55.029	28.582	0.172	10.517	5.311	0.494	100.105	2.480	1.518	0.006	0.508	0.464	0.028	13.005	$An_{50.8}Ab_{46.4}Or_{2.8}$
	54.050	29.010	0.121	10.805	5.350	0.513	99.850	2.448	1.549	0.005	0.524	0.470	0.030	13.026	$An_{51.2}Ab_{45.9}Or_{2.9}$

Sample															
	54.717	28.739	0.127	10.636	5.273	0.487	99.981	2.470	1.529	0.005	0.515	0.462	0.028	13.009	$An_{51.2}Ab_{46.0}Or_{2.8}$
	54.141	28.695	0.090	10.649	5.318	0.509	99.403	2.461	1.537	0.003	0.519	0.469	0.030	13.018	$An_{51.0}Ab_{46.1}Or_{2.9}$
	53.816	28.468	0.027	10.609	5.293	0.484	98.697	2.463	1.535	0.001	0.520	0.470	0.028	13.017	$An_{51.1}Ab_{46.1}Or_{2.8}$
	55.160	29.055	0.090	10.641	5.273	0.483	100.702	2.471	1.534	0.003	0.511	0.458	0.028	13.004	$An_{51.3}Ab_{46.0}Or_{2.8}$
MAD-blue	55.655	28.276	0.063	9.924	5.492	0.536	99.947	2.506	1.501	0.002	0.479	0.479	0.031	12.999	$An_{48.6}Ab_{48.5}Or_{3.1}$
	55.153	27.853	0.117	10.018	5.339	0.474	98.956	2.509	1.493	0.004	0.488	0.471	0.028	12.994	$An_{49.5}Ab_{47.7}Or_{2.8}$
	55.506	28.283	0.123	10.290	5.524	0.423	100.150	2.497	1.500	0.004	0.496	0.482	0.024	13.004	$An_{49.5}Ab_{48.1}Or_{2.4}$
	55.757	28.376	0.117	10.235	5.543	0.435	100.463	2.500	1.499	0.004	0.492	0.482	0.025	13.002	$An_{49.2}Ab_{48.3}Or_{2.5}$
	56.331	28.234	0.110	10.260	5.599	0.405	100.939	2.512	1.484	0.004	0.490	0.484	0.023	12.997	$An_{49.1}Ab_{48.5}Or_{2.3}$
	55.467	28.445	0.114	10.307	5.661	0.423	100.417	2.491	1.505	0.004	0.496	0.493	0.024	13.013	$An_{49.0}Ab_{48.7}Or_{2.4}$
R2923-red	54.958	27.991	0.045	10.785	5.06	0.467	99.305	2.495	1.498	0.002	0.525	0.445	0.027	12.992	$An_{52.6}Ab_{44.7}Or_{2.7}$
	54.24	28.24	0.03	11.22	5.263	0.427	99.419	2.468	1.514	0.001	0.547	0.464	0.025	13.019	$An_{52.8}Ab_{44.8}Or_{2.4}$
	54.007	28.089	0.149	10.883	5.32	0.459	98.907	2.47	1.514	0.006	0.533	0.472	0.027	13.022	$An_{51.7}Ab_{45.7}Or_{2.6}$
	53.567	28.201	0.095	11.13	5.187	0.44	98.619	2.459	1.526	0.004	0.547	0.462	0.026	13.022	$An_{52.9}Ab_{44.6}Or_{2.5}$
R2923-blue	54.381	27.900	0.260	10.364	5.314	0.442	98.661	2.488	1.505	0.010	0.508	0.471	0.026	13.008	$An_{50.5}Ab_{46.9}Or_{2.6}$
	54.599	27.987	0.292	10.343	5.299	0.464	98.983	2.490	1.504	0.011	0.505	0.469	0.027	13.006	$An_{50.5}Ab_{46.8}Or_{2.7}$
	54.420	27.903	0.281	10.379	5.365	0.414	98.763	2.488	1.503	0.011	0.508	0.476	0.024	13.010	$An_{50.4}Ab_{47.2}Or_{2.4}$
	54.473	27.940	0.177	10.365	5.369	0.430	98.755	2.489	1.505	0.007	0.507	0.476	0.025	13.009	$An_{50.3}Ab_{47.2}Or_{2.5}$
Gem113-Blue	55.292	28.591	0.342	10.898	5.151	0.404	100.677	2.480	1.512	0.013	0.524	0.448	0.023	13.000	$An_{52.6}Ab_{45.0}Or_{2.3}$
	56.138	28.399	0.339	10.734	5.261	0.431	101.302	2.500	1.491	0.013	0.512	0.454	0.024	12.994	$An_{51.7}Ab_{45.8}Or_{2.5}$
	55.831	28.283	0.251	11.039	5.235	0.417	101.056	2.495	1.489	0.009	0.528	0.454	0.024	12.999	$An_{52.5}Ab_{45.1}Or_{2.4}$

	56.070	28.427	0.319	11.024	5.180	0.394	101.413	2.496	1.491	0.012	0.526	0.447	0.022	12.994	$An_{52.8}Ab_{44.9}Or_{2.2}$
	55.559	28.835	0.299	11.073	5.216	0.404	101.387	2.476	1.514	0.011	0.529	0.451	0.023	13.004	$An_{52.7}Ab_{45.0}Or_{2.3}$
	55.716	28.590	0.302	10.869	5.133	0.391	101.002	2.489	1.505	0.011	0.520	0.445	0.022	12.992	$An_{52.7}Ab_{45.0}Or_{2.3}$
Gem113 -red	55.250	28.516	0.251	11.097	4.722	0.408	100.244	2.485	1.512	0.009	0.535	0.412	0.023	12.976	$An_{55.1}Ab_{42.5}Or_{2.4}$
	55.446	28.348	0.234	11.157	4.956	0.607	100.748	2.487	1.499	0.009	0.536	0.431	0.035	12.996	$An_{53.5}Ab_{43.0}Or_{3.5}$
	55.343	28.338	0.289	10.954	4.986	0.344	100.255	2.490	1.503	0.011	0.528	0.435	0.020	12.986	$An_{53.7}Ab_{44.3}Or_{2.0}$
	55.472	28.477	0.337	11.216	4.936	0.401	100.839	2.484	1.503	0.013	0.538	0.429	0.023	12.990	$An_{54.4}Ab_{43.3}Or_{2.3}$
	54.426	28.053	1.810	10.875	4.886	0.405	100.454	2.465	1.498	0.069	0.528	0.429	0.023	13.012	$An_{53.8}Ab_{43.8}Or_{2.4}$
	55.650	28.183	0.259	11.215	4.982	0.418	100.707	2.495	1.489	0.010	0.539	0.433	0.024	12.989	$An_{54.1}Ab_{43.5}Or_{2.4}$
Gem118 -red	53.710	28.070	0.196	11.589	4.471	0.438	98.474	2.466	1.519	0.008	0.570	0.398	0.026	12.986	$An_{57.4}Ab_{40.1}Or_{2.6}$
	54.061	28.523	0.288	11.841	4.435	0.508	99.656	2.456	1.527	0.011	0.576	0.391	0.029	12.990	$An_{57.8}Ab_{39.2}Or_{3.0}$
	53.739	28.836	0.296	11.906	4.438	0.473	99.689	2.442	1.544	0.011	0.580	0.391	0.027	12.995	$An_{58.1}Ab_{39.2}Or_{2.7}$
	54.128	28.567	0.256	11.965	4.497	0.527	99.940	2.454	1.526	0.010	0.581	0.395	0.030	12.996	$An_{57.7}Ab_{39.3}Or_{3.0}$
	54.123	28.798	0.318	11.892	4.180	0.457	99.768	2.453	1.538	0.012	0.578	0.367	0.026	12.975	$An_{59.5}Ab_{37.8}Or_{2.7}$
	54.122	28.840	0.303	11.699	4.448	0.408	99.820	2.452	1.540	0.011	0.568	0.391	0.024	12.985	$An_{57.8}Ab_{39.8}Or_{2.4}$
Gem118 -blue	53.447	28.059	0.266	11.322	4.733	0.522	98.348	2.461	1.522	0.010	0.558	0.422	0.031	13.005	$An_{55.2}Ab_{41.8}Or_{3.0}$
	54.656	27.652	0.238	11.530	4.825	0.692	99.594	2.486	1.482	0.009	0.562	0.426	0.040	13.005	$An_{54.7}Ab_{41.4}Or_{3.9}$
	53.801	27.638	0.251	11.224	4.690	0.533	98.136	2.480	1.501	0.010	0.554	0.419	0.031	12.995	$An_{55.2}Ab_{41.7}Or_{3.1}$
	54.151	27.729	0.278	11.165	4.797	0.495	98.615	2.483	1.498	0.011	0.549	0.426	0.029	12.996	$An_{54.6}Ab_{42.5}Or_{2.9}$

Table S2 Intensity ratios from TEM-EDS spectrum of individual lamellae and the calibrated An# based on bulk composition and volume ratio between lamellae. The An# bulk is fixed from the EPMA analyses, and the *k*-factor is calculated by fitting the volume ratio to the predetermined number (2:1 for red area and 1:1 for blue area).

Sample	$\frac{I_{Ca}}{I_{Na}}$ of Ca-rich lamella	$\frac{I_{Ca}}{I_{Na}}$ of Na-rich lamella	k	An# Ca-rich lamella	An# Na-rich lamella	An# Diff.	An# Bulk	Volume Ratio $\frac{Ca-rich}{Na-rich}$
R2923 -red	2.860	1.922	2.27	55.7	45.8	9.9	52.5	2.0
	2.916	1.958	2.31	55.8	45.9	9.9	52.5	2.0
	3.140	2.080	2.47	56.0	45.7	10.3	52.5	2.0
	3.052	2.087	2.43	55.7	46.2	9.5	52.5	2.0
	3.085	2.103	2.46	55.6	46.1	9.5	52.5	2.0
R2923 -blue	2.672	1.603	2.03	56.8	44.1	12.7	50.5	1.0
	2.691	1.495	1.96	57.9	43.3	14.6	50.5	1.0
	2.746	1.482	1.98	58.1	42.8	15.3	50.5	1.0
	2.824	1.525	2.03	58.2	42.9	15.3	50.5	1.0
Gem113 -red	2.047	1.417	1.54	57.1	47.9	9.2	54.0	2.0
	2.095	1.476	1.59	56.8	48.1	8.7	54.0	2.1
	1.809	1.252	1.36	57.1	47.9	9.2	54.0	2.0
	1.867	1.319	1.42	56.8	48.2	8.7	54.0	2.1
	1.351	0.905	1.01	57.2	47.3	10.0	54.0	2.1
	1.367	0.882	1.01	57.5	46.6	10.9	54.0	2.1
	1.371	0.911	1.02	57.3	47.2	10.2	54.0	2.0
Gem113 -blue	1.244	0.700	0.86	59.1	44.9	14.2	52.0	1.0
	1.251	0.706	0.87	59.0	44.8	14.2	52.0	1.0
	1.150	0.658	0.80	59.0	45.1	13.9	52.0	1.0
VB -yellow	2.439	1.508	1.70	58.9	47.0	11.9	55.0	2.0
	2.523	1.710	1.81	58.2	48.6	9.7	55.0	2.0
	2.667	1.776	1.90	58.4	48.3	10.1	55.0	2.0
	2.531	1.682	1.80	58.4	48.3	10.1	55.0	1.9
	2.889	1.847	2.03	58.7	47.6	11.1	55.0	2.0
	3.170	1.967	2.21	58.9	47.1	11.8	55.0	2.0
	3.078	2.111	2.22	58.1	48.7	9.4	55.0	2.0
Gem118 -red	3.988	2.228	2.37	62.7	48.5	14.3	58.0	2.0
	3.908	2.214	2.33	62.6	48.7	13.9	58.0	2.0
	3.616	1.922	2.11	63.2	47.7	15.5	58.0	2.0
	3.500	1.854	2.04	63.2	47.6	15.5	58.0	2.0
Gem118 -blue	3.510	1.913	2.11	62.5	47.5	14.8	55.0	1.0
	3.479	1.976	2.14	61.9	48.0	13.9	55.0	1.0
	3.853	2.026	2.27	62.9	47.2	15.8	55.0	1.0
	4.167	2.254	2.49	62.6	47.5	15.1	55.0	1.0
	4.240	2.291	2.54	62.5	47.4	15.1	55.0	1.0

	4.569	2.461	2.73	62.6	47.4	15.2	55.0	1.0

References

Carpenter, M. A. (1994) Subsolidus phase-relations of the plagioclase feldspar solid-solution. In Ian Parsons, Ed., Feldspars and Their Reactions Vol. 421, pp. 221–269. Kluwer Academic Publishers, Netherlands.

Grove, T. L., Ferry, J. M., and Spear, F. S. (1983) Phase transitions and decomposition relations in calcic plagioclase. American Mineralogist, 68, 41-59.

Grove, T. L., Ferry, J. M., and Spear, F. S. (1986) Phase transitions in calcic plagioclase; a correction and further discussion. American Mineralogist, 71, 1049-1050.

McConnell, J. D. C. (1974) Electron-optical study of the fine structure of a schiller labradorite. In W.S. MacKenzie and J. Zussman, Eds., The Feldspars pp. 478–490. Manchester University Press, New York.

McConnell, J. D. C. (2008) The origin and characteristics of the incommensurate structures in the plagioclase feldspars. The Canadian Mineralogist, 46, 1389-1400.

Nord, G. L., Heuer. A. H, and Lally, J. S. (1974) Transmission electron microscopy of substructures in Stillwater bytownite. In W. S. MacKenzie and J. Zussman, Eds., The Feldspars, p. 522- 535. Manchester University Press, New York.

Ribbe, P.H. (1987) McGraw-Hill Encyclopedia of Science & Technology: An International Reference Work in Twenty Volumes Including an Index Vol. 7, pp. 38–47. McGraw-Hill, New York.

Smith, J. V. (1974). Feldspar Minerals, 692 p. Springer-Verlag, Berlin, New York.

Smith, J. V. (1984). Phase relations of plagioclase feldspars. In W. L. Brown, Eds., Feldspars and

  feldspathoids, p. 55-94. Springer, Netherlands.

Vinograd, V. L., Putnis, A., and Kroll, H. (2001) Structural discontinuities in plagioclase and constraints

  on mixing properties of the low series: A computational study. Mineralogical Magazine, 65, 1-31.